LETTERS
PUBLISHED ONLINE: 27 SEPTEMBER 2009 | DOI: 10.1038/NNANO.2009.276
nature nanotechnology

Programming the detection limits of biosensors through controlled nanostructuring

Leyla Soleymani[1], Zhichao Fang[2], Edward H. Sargent[1]* and Shana O. Kelley[2,3]*

Advances in materials chemistry offer a range of nanostructured shapes and textures for building new biosensors[1–10]. Previous reports have implied that controlling the properties of sensor substrates can improve detection sensitivities, but the evidence remains indirect[11–13]. Here we show that by nanostructuring the sensing electrodes, it is possible to create nucleic acid sensors that have a broad range of sensitivities and that are capable of rapid analysis. Only highly branched electrodes with fine structuring attained attomolar sensitivity. Nucleic acid probes immobilized on finely nanostructured electrodes appear more accessible and therefore complex more rapidly with target molecules in solution. By forming arrays of microelectrodes with different degrees of nanostructuring, we expanded the dynamic range of a sensor system from two to six orders of magnitude. The demonstration of an intimate link between nanoscale sensor structure and biodetection sensitivity will aid the development of high performance diagnostic tools for biology and medicine.

To explore the role of nanostructuring in the performance of biosensors, we designed a device architecture that would allow the response of many different sensors to be evaluated in parallel on a single chip. We produced a wide range of nanostructured elements on this chip so the response of different sensors challenged with the same sample could be evaluated in parallel. The planar chip has multiple electrically independent gold leads (Fig. 1a). The leads were passivated with silicon dioxide and at the tip of each lead were apertures with 500 nm diameters. Using metal electrodeposition[5,14,16] under a wide range of plating conditions, we generated a variety of differently nanostructured palladium electrodes in the apertures to complete the microelectrode array. The strong binding affinity of palladium for thiols[15] enabled us to functionalize and attach biomolecular probes on the nanostructured microelectrodes (NMEs), which were remarkably reproducible, robust and programmable.

Figures 1 and 2 show how the nanostructure size and topography is programmed using the axes of time, electroplating potential, reagent concentration and supporting electrolytes. When low potentials were used, very smooth microelectrodes were generated (Fig. 1b); at higher potentials, microelectrodes with extensive nanostructuring were produced. Increasing the plating potential accelerates the electrodeposition kinetics, promoting rougher structures where growth proceeds outwards faster than internal voids can be filled in. The supporting electrolyte used for electrodeposition also exerted a significant effect on microelectrode nanostructuring (Fig. 1c–e). Deposition in the presence of hydrochloric acid produced structures that were dense and nanorough on the scale of 100–300 nm, whereas when $HClO_4$ was used, or in the absence of an electrolyte, finer structures nanorough on the scale of 20–50 nm were produced. HCl is an inhibitory electrolyte that slows the growth of the NMEs by suppressing the ionization of the palladium(II) salt. However, when $HClO_4$ is used as an electrolyte, growth proceeds without inhibition and the fast electrodeposition that is therefore observed yields more fractal structures as the growth of tree-like structures occurs efficiently.

These electrodes exhibit ideal microelectrode behaviour (Fig. 2c), and maximize current density and signal magnitude while keeping the surface area small. Importantly, the fabrication of these electrodes was highly reproducible (Supplementary Fig. S1, Supplementary Information), with microelectrodes consistently exhibiting working areas that differed by less than 15%.

We explored how nanostructuring influenced the sensitivity of a nucleic acid assay using a chip containing these diversely structured electrodes. We used an electrocatalytic reporter system previously developed by our laboratories (Fig. 3a)[11,17–19] for this study. Electrocatalysis provides electronic amplification, or gain, facilitating high-sensitivity readout: hundreds of electrons flow as a result of each biomolecular complexation event. In our system, the primary electron acceptor $Ru(NH_3)_6^{3+}$ is electrostatically attracted to the electrode surface in proportion to the amount of bound nucleic acid. When $Fe(CN)_6^{3-}$ is used during electrochemical readout the Ru(III) substrate is regenerated because the Fe(III) species is even easier to reduce; but as it is electrostatically repelled from the electrode, $Fe(CN)_6^{3-}$ only undergoes chemical reduction by Ru(II). This method is label-free and does not require the sample to be processed in any way—an important feature for a practical device. To impart maximal sensitivity to the assay, we incorporated an additional component into the assay—peptide nucleic acid (PNA) probes. Long known to exhibit higher affinity to a complementary sequence than DNA or RNA[20,21], peptide nucleic acid has been shown to possess an additional advantage for use with our electrocatalytic readout system[17]. Given that peptide nucleic acids are charge-neutral, electrocatalysis will not occur with single-stranded neutral probes on the electrode surface, thus almost no signal is observed until target nucleic acid is bound to the surface.

Sensing elements with varied degrees of nanostructuring exhibited dramatically different responses to a given analyte at a given concentration (Fig. 3b,c). We measured the limits of detection and the dynamic ranges of a smooth sphere microelectrode, a moderately nanorough NME and a finely nanorough NME (Fig. 2 and Fig. 4). The limits of detection observed with these structures were dramatically influenced by the fineness of the nanostructuring: for finely nanostructured microelectrode sensors the limit of detection was 10 aM, for the moderately nanostructured sensors it was 10 fM, and for the smooth structures, 100 fM. The experiments reported in Fig. 4 alone involved the analysis of more than 100 different devices, highlighting that the fabrication method developed is robust.

[1]Department of Electrical and Computer Engineering, Faculty of Engineering, [2]Department of Pharmaceutical Sciences, Leslie Dan Faculty of Pharmacy, [3]Department of Biochemistry, Faculty of Medicine, University of Toronto, Toronto, Ontario, Canada. *e-mail: shana.kelley@utoronto.ca; ted.sargent@utoronto.ca

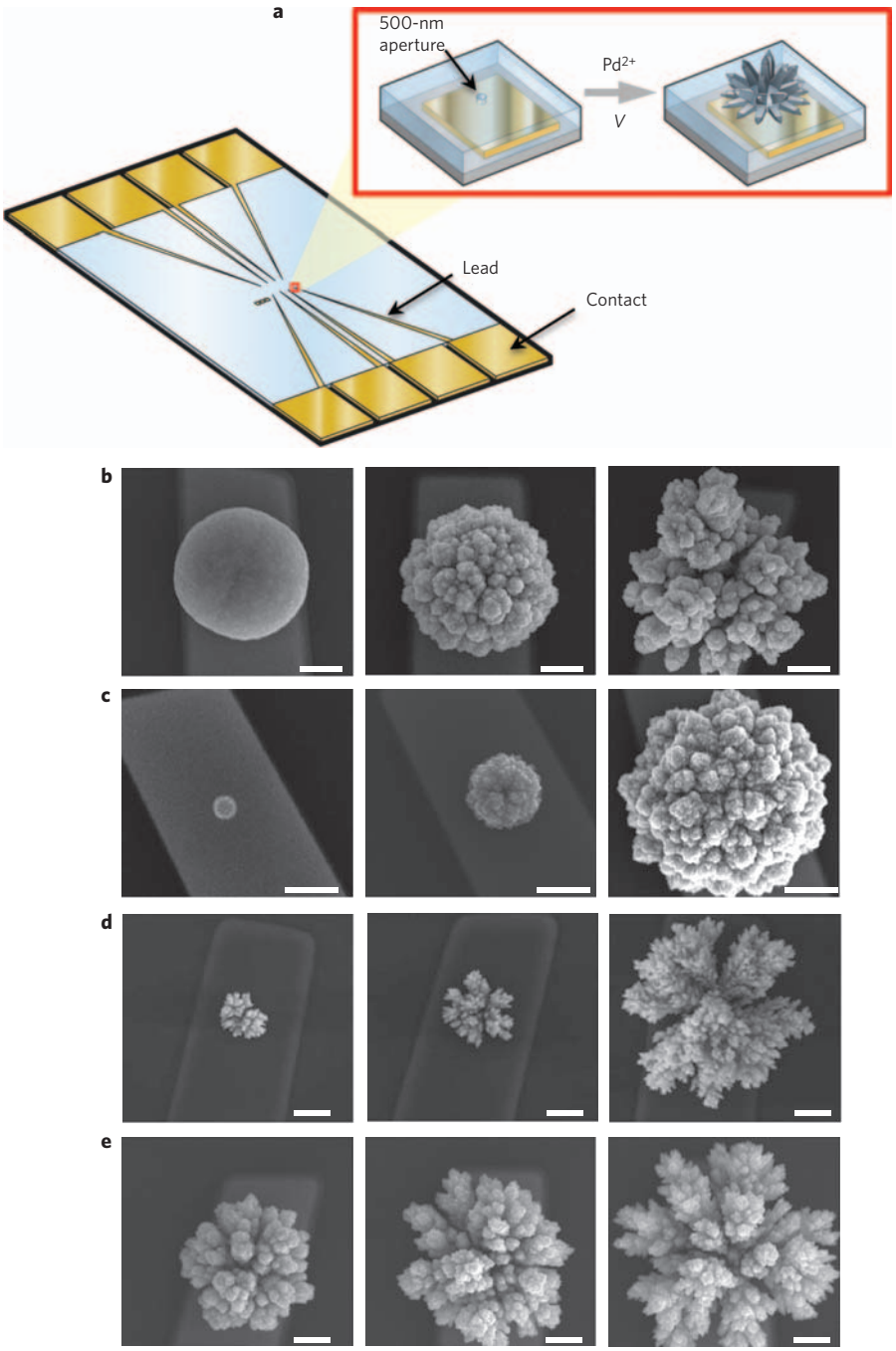

Figure 1 | Programmable NMEs. a, Top-down template fabrication. A gold pattern of electrical leads deposited on a silicon wafer using conventional photolithography is covered with a layer of SiO_2. 500-nm apertures etched through this top layer expose a circular section of gold. Large square pads are used as external contacts. Inset: bottom-up deposition of sensing elements. The schematic illustrates electrodeposition of metal electrodes in the apertures. **b-e**, Scanning electron microscope images illustrating the effect of deposition parameters on nanostructuring. **b**, Larger plating potential creates more extensive nanostructures. Structures are fabricated (from left) at 0 mV, -100 mV and -250 mV in HCl for 150 s. **c**, Effect of deposition time on the structure size. The same aperture is imaged (from left) after 20, 125 and 500 seconds of plating at -100 mV in HCl. **d**, Effect of deposition time and supporting electrolyte on plating rate. Structures are plated in $HClO_4$ as supporting electrolyte at -100 mV for (from left) 5 s, 10 s and 40 s. **e**, Effect of palladium ion/supporting electrolyte ratio on NME morphology. Structures are fabricated (from left) in 5 mM H_2PdCl_4 + 0.060 M HCl, 5 mM H_2PdCl_4 + 0.030 M HCl, 5 mM H_2PdCl_4 + 0.015 M HCl, at -100 mV for 150 s. All scale bars correspond to 2 μm.

Because the three types of structures, which can be generated on a single chip, were responsive in distinct concentration regimes, their multiplexing can be used to realize a dynamic range of six to seven orders of magnitude. This feature is not available in other array-based platforms that have access to only a single type of sensor nanostructure[12,13]. Expanded dynamic range is a powerful tool for the monitoring of disease-associated nucleic acids, such as cancer-related genes, which are known to vary over many orders of magnitude in patient samples[22].

We investigated two hypotheses aimed at exploring the physical mechanisms of the enhanced sensitivity in the most finely nanostructured devices: that increased surface area of the nanostructured electrodes enhances redox currents relative to smooth structures,

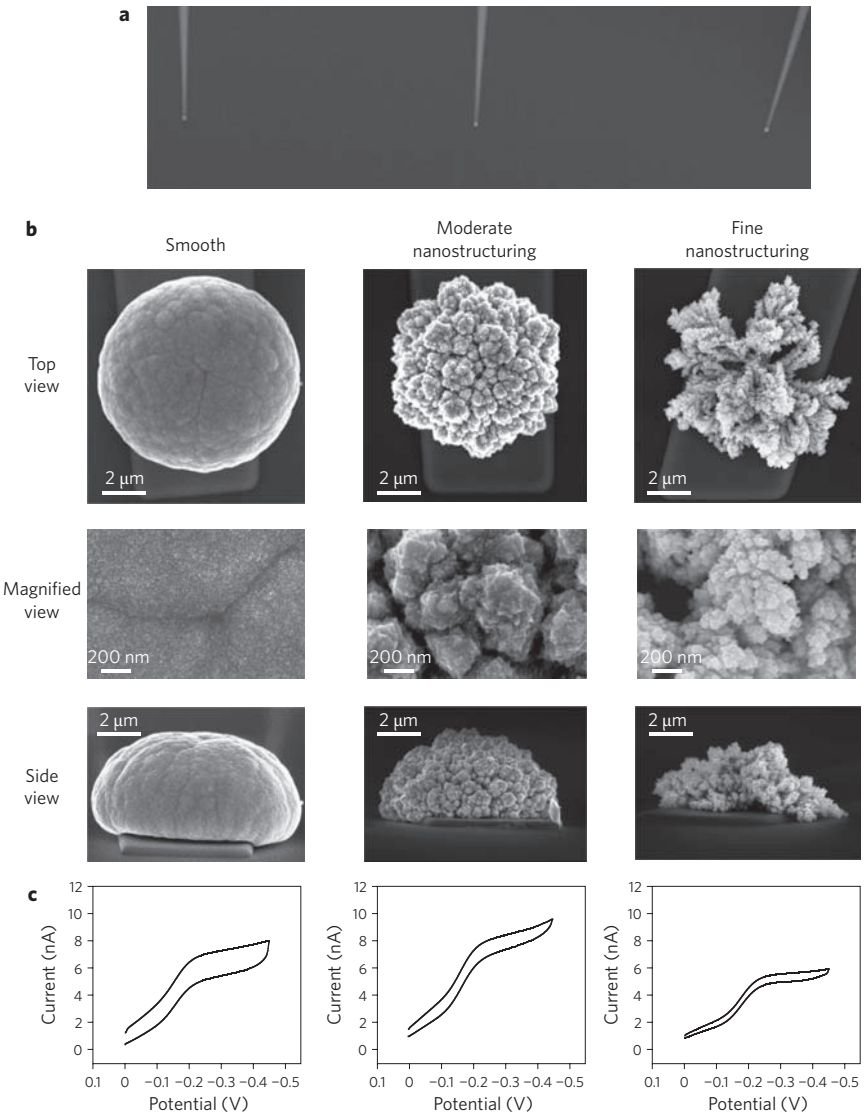

Figure 2 | Comparison of NMEs with diverse nanostructuring. a,**b**, Pd NMEs produced with different levels of nanotexturing on the same chip. Scanning electron microscope image in **a** shows three leads on the same chip that display the three different types of NMEs shown in **b**. The three NMEs have significantly different surface structures: smooth, moderately nanostructured, and finely nanostructured. **c**, Comparison of solution electrochemistry for a 3 mM $Ru(NH_3)_6^{3+}$ solution at smooth (left), moderate (middle) and finely (right) nanostructured microelectrodes. Electrochemistry was monitored as described in the Methods section.

and improves sensitivity (the area hypothesis); and that the surface textures of nanostructured electrodes enhances accessibility during hybridization, leading to faster and more efficient binding of the analyte (the accessibility hypothesis). To evaluate the area hypothesis, we measured the working area of each differently nanostructured electrode using the type of electrochemical data shown in Fig. 2c. We found that the more finely nanostructured NMEs had smaller apparent working areas than the less nanostructured electrodes, and that the finer nanostructuring did not produce enhanced mass transport. Indeed, smaller currents were observed when solution-borne species such as $Ru(NH_3)_6^{3+}$ were monitored at bare highly nanostructured NMEs, indicating that only the outer layer of nanostructures may collect electrochemical signals. The metal facets on the interior of the fractal-like NME may limit heterogeneous electron transfer. In addition, the diffusion layer of redox reagents may be consumed by the outer layer of nanostructures.

We then sought to examine the accessibility hypothesis: that incorporating nanoscale structural features into sensing elements results in the display of probe molecules in a more favourable conformation for hybridization, promoting more efficient complexation with the target sequence. The observation that finely nanotextured NMEs, with features ranging from 20–50 nm, had a limit of detection three orders of magnitude lower than NMEs with moderate (100–300 nm) nanostructuring, could be the result of such an effect. To evaluate this hypothesis, we monitored directly the kinetics of hybridization at two differently nanostructured biosensing electrodes. The results are shown in Fig. 5. The more nanostructured sensor exhibited a very fast response, rising to 70% of its maximal signal within two minutes. The coarser, denser structure took significantly longer to generate the same signal change, indicating that hybridization is slower when probes are displayed on this structure. The results suggest that immobilized biomolecules with length scales of 5–10 nm are more accessible when displayed on structures that are finely featured on a similar length scale.

The 10 aM sensitivity achieved herein using our optimized NMEs and electrocatalytic reporter system is the lowest detection limit reported to date for a label- and polymerase chain reaction (PCR)-free sensor. This limit corresponds to the detection of

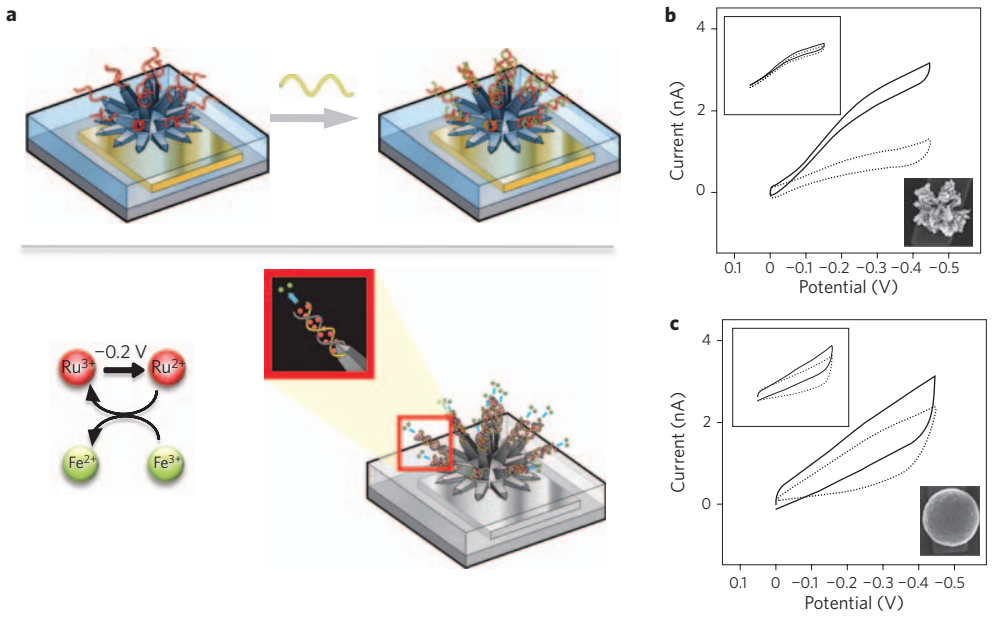

Figure 3 | Electrocatalytic nucleic acid detection at NMEs. a, Electrocatalytic reporter assay for nucleic acid hybridization. The presence of a target sequence is transduced using an electrocatalytic Ru(III)/Fe(III) reporter system and is read using measurements of electrochemical current. **b**,**c**, Sensitivity of a PNA-modified finely nanostructured (**b**) and smooth (**c**) NME to hybridization (dotted line, pre-hybridization signal; solid line, post-hybridization signal) with a solution containing 100 aM of a complementary target sequence as monitored by the electrocatalytic reporter assay. Insets in **b** and **c** show the change in signal when a 100 fM non-complementary target was introduced. These plots have the same scale as those for the complementary targets.

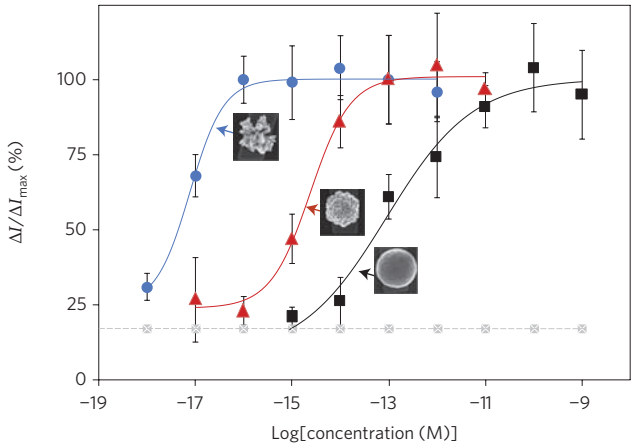

Nanostructuring length scale	None	100–300 nm	20–50 nm
Detection limit	100 fM	10 fM	10 aM
Log-linear dynamic range	10 fM–10 pM	100 aM–10 fM	1 aM–100 aM

Figure 4 | Comparison of the detection limit and dynamic range of three probe-modified Pd NMEs with different levels of nanostructuring. ΔI values were read out from currents collected in cyclic voltammetry sweeps performed as shown in Fig. 3 and as described in the Methods section. Data represent averages from six to eight trials. The probe sequence used in these experiments is PNA probe 1P, and the target sequence 1T was hybridized as described in the Methods section. The error shown is the standard error; 100 fM of a non-complementary sequence (seq. 1C) was used as a control to evaluate background levels (average background shown as grey line). Device responses were normalized to the plateau currents.

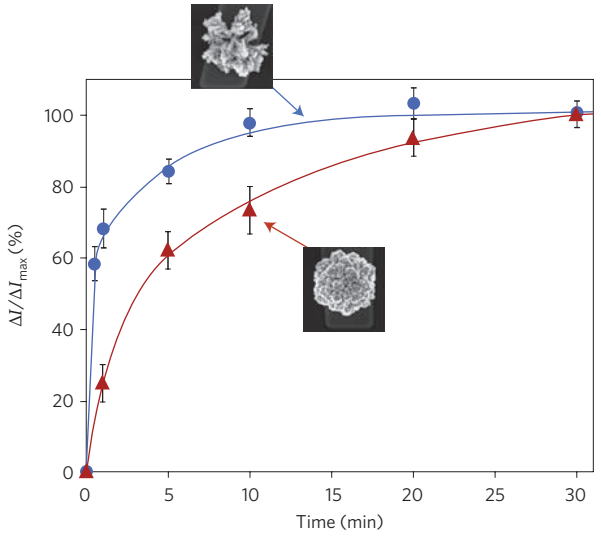

Figure 5 | Hybridization kinetics observed for two different types of NMEs. NMEs with moderate (red) and fine (blue) nanostructuring were studied by measuring the time evolution of ΔI while immersing the PNA-modified NMEs in solutions containing 100 fM of synthetic target and the Ru(III)/Fe(III) reporter groups.

fewer than 100 copies of the target sequence. The measurement of 60–1,000 copies of target sequence was previously reported based on electrochemical detectors exploiting multistep catalytic readout[23,24]; and multiplexed electronic chips have been generated previously for nucleic acid detection[12,13,25]. However, the sensitivity reported here has never been achieved on a chip-based platform using single-step readout.

Our findings prove that reproducible, rationally controlled growth of diverse nanostructures integrated onto a chip may be implemented using top-down-programmed, bottom-up-implemented, nanotechnology. Because nanostructuring on the biomolecular length

scale can influence sensitivity, as proven herein, this controlled integration of nanomaterials provides a major advantage in biomolecular detection.

Methods

Chip fabrication. The chips were fabricated at the Canadian Photonics Fabrication Center. Three-inch silicon wafers were passivated using a thick layer of thermally grown silicon dioxide. A 350-nm gold layer was deposited on the chip using electron-beam-assisted gold evaporation. The gold film was patterned using standard photolithography and a lift-off process. A 500-nm layer of insulating silicon dioxide was deposited using chemical vapour deposition. 500-nm apertures were imprinted on the electrodes using standard photolithography, and 2×2 mm bond pads were exposed using standard photolithography.

Fabrication of nanostructured microelectrodes. Chips were cleaned by rinsing in acetone, isopropanol and deionized water for 30 s and dried with a flow of nitrogen. All electrodeposition was performed at room temperature with a Bioanalytical Systems Epsilon potentiostat with a three-electrode system featuring an Ag/AgCl reference electrode and a platinum wire auxiliary electrode. 500-nm apertures on the fabricated electrodes were used as the working electrode and were contacted using the exposed bond pads. H_2PdCl_4 was synthesized by reacting palladium(II) chloride and hydrochloric acid. All structures presented in Fig. 2 were deposited using the settings described in the figure captions using d.c. potential amperometry in a three-electrode setup with Ag/AgCl serving as a reference electrode.

Preparation and purification of oligonucleotides. All synthetic oligonucleotides were stringently purified by reversed-phase high-performance liquid chromatography. The following probe and target sequences were used in experiments: seq. 1P, peptide nucleic acid probe: NH_2-Cys-Gly-ATA AGG CTT CCT GCC GCG CT-$CONH_2$; seq. 1T, complementary DNA target: $^{5'}$AGC GCG GCA GGA AGC CTT AT$^{3'}$; seq. 1C, non-complementary DNA target: $^{5'}$TTT TTT TTT TTT TTT TTT TT$^{3'}$ Oligonucleotides were quantitated by measuring absorbance at 260 nm and extinction coefficients calculated using http://www.idtdna.com/analyser/Applications/OligoAnalyser/.

Modification of NMEs with peptide nucleic acid probes. A solution containing 500 nM thiolated single-stranded peptide nucleic acid, 25 mM sodium phosphate (pH 7) and 25 mM sodium chloride was heated at 50 °C for 10 minutes. A suitable amount of 10 μM mercaptohexanol (MCH) was then added to make the final MCH concentration of 100 nM. 0.5–10 μl (depending on the degree of multiplexing) of this mixture was deposited on the NMEs in a dark humidity chamber overnight at 4 °C. Each chip featured eight individually addressable NMEs, and so probes were individually spotted on each NME according to the sequence to be detected. This spotting was done using a manual micropipette. The NMEs were rinsed in 25 mM sodium phosphate (pH 7) and 25 mM NaCl buffer before measurements.

Electrochemical measurements. Electrochemical signals were measured in solutions containing 10 μM $Ru(NH_3)_6^{3+}$, 25 mM sodium phosphate (pH 7), 25 mM sodium chloride and 4 mM $Fe(CN)_6^{3-}$. Cyclic voltammetry signals before and after hybridization were collected with a scan rate of 100 mV s^{-1}. Limiting reductive current (I) was quantified by subtracting the background at 0 mV from the cathodic current at –300 mV in a cyclic voltammetry signal. Signal changes corresponding to hybridization were calculated as follows: $\Delta I = (I_{ds} - I_{ss})/I_{ss} \times 100$ (ss = before hybridization, ds = after hybridization), and normalized to the maximal response of a specific device type. The detection limit was defined as the first concentration for which the background (non-complementary ΔI)-subtracted signal was three times higher than the standard deviation at that concentration.

Hybridization protocol. Hybridization solutions typically contained target sequences in 25 mM sodium phosphate (pH 7) and 25 mM NaCl. Electrodes were incubated at 37 °C in a humidity chamber in the dark for 60 minutes and were washed extensively with buffer before electrochemical analysis. Hybridization was performed in 10 μl volumes.

Kinetic measurements of DNA hybridization at NMEs. NMEs modified with peptide nucleic acid were prepared as described above. Rinsed NMEs were immersed in a solution containing 10 μM $Ru(NH_3)_6^{3+}$, 4 mM $Fe(CN)_6^{3-}$, 100 fM DNA target (seq. 4), 25 mM sodium phosphate (pH 7) and 25 mM NaCl. The electrocatalytic cyclic voltammetry signals were obtained as described above. All measurements were performed at 37 °C.

Received 29 June 2009; accepted 20 August 2009; published online 27 September 2009

References

1. Aizawa, M. & Buriak, J. M. Nanoscale patterning of two metals on silicon surfaces using an ABC triblock copolymer template. *J. Am. Chem. Soc.* **128,** 5877–5886 (2006).
2. Chai, J., Wang, D., Fan, X. & Buriak, J. M. Assembly of aligned linear metallic patterns on silicon. *Nature Nanotech.* **2,** 500–506 (2007).
3. Cui, Y. & Lieber, C. M. Functional nanoscale electronic devices assembled using silicon nanowire building blocks. *Science* **291,** 851–853 (2001).
4. Henzie, J. *et al.* Nanofabrication of plasmonic structures. *Annu. Rev. Phys. Chem.* **60,** 147–165 (2009).
5. Kline, T. R. *et al.* Template-grown metal nanowires. *Inorg. Chem.* **45,** 7555–7565 (2006).
6. LeMieux, M. C. *et al.* Self-sorted, aligned nanotube networks for thin-film transistors. *Science* **321,** 101–104 (2008).
7. Lu, W. & Lieber, C. M. Nanoelectronics from the bottom up. *Nature Mater.* **6,** 841–850 (2007).
8. Mirkovic, T. *et al.* Hinged nanorods made using a chemical approach to flexible nanostructures. *Nature Nanotech.* **2,** 565–569 (2007).
9. Nicewarner-Pena, S. R. *et al.* Submicrometer metallic barcodes. *Science* **294,** 137–141 (2001).
10. Zhu, J. *et al.* Optical absorption enhancement in amorphous silicon nanowire and nanocone arrays. *Nano Lett.* **9,** 279–282 (2009).
11. Gasparac, R. *et al.* Ultrasensitive electrocatalytic DNA detection at two- and three-dimensional nanoelectrodes. *J. Am. Chem. Soc.* **126,** 12270–12271 (2004).
12. Hahm, J. & Lieber, C. M. Direct ultrasensitive electrical detection of DNA and DNA sequence variations using nanowire nanosensors. *Nano Lett.* **4,** 51–54 (2004).
13. Park, S. J., Taton, T. A. & Mirkin, C. A. Array-based electrical detection of DNA with nanoparticle probes. *Science* **295,** 1503–1506 (2002).
14. Lahav, M., Weiss, E. A., Xu, Q. & Whitesides, G. M. Core-shell and segmented polymer-metal composite nanostructures. *Nano Lett.* **6,** 2166–2171 (2006).
15. Love, J. C. *et al.* Formation and structure of self-assembled monolayers of alkanethiolates on palladium. *J. Am. Chem. Soc.* **125,** 2597–2609 (2003).
16. LaVan, D. A., George, P. M. & Langer, R. Simple, three-dimensional microfabrication of electrodeposited structures. *Angew. Chem. Int. Ed.* **42,** 1262–1265 (2003).
17. Fang, Z. & Kelley, S. O. Direct electrocatalytic mRNA detection using PNA-nanowire sensors. *Anal. Chem.* **81,** 612–617 (2009).
18. Lapierre, M. A., O'Keefe, M., Taft, B. J. & Kelley, S. O. Electrocatalytic detection of pathogenic DNA sequences and antibiotic resistance markers. *Anal. Chem.* **75,** 6327–6333 (2003).
19. Lapierre-Devlin, M. A. *et al.* Amplified electrocatalysis at DNA-modified nanowires. *Nano Lett.* **5,** 1051–1055 (2005).
20. Egholm, M. *et al.* PNA hybridizes to complementary oligonucleotides obeying the Watson-Crick hydrogen-bonding rules. *Nature* **365,** 566–568 (1993).
21. Ratilainen, T. *et al.* Thermodynamics of sequence-specific binding of PNA to DNA. *Biochemistry* **39,** 7781–7791 (2000).
22. Ludwig, J. A. & Weinstein, J. N. Biomarkers in cancer staging, prognosis and treatment selection. *Nat. Rev. Cancer* **5,** 845–856 (2005).
23. Munge, B., Liu, G. D., Collins, G. & Wang, J. Multiple enzyme layers on carbon nanotubes for electrochemical detection down to 80 DNA copies. *Anal. Chem.* **77,** 4662–4666 (2005).
24. Zhang, Y. C., Pothukuchy, A., Shin, W., Kim, Y. & Heller, A. Detection of similar to 10^3 copies of DNA by an electrochemical enzyme-amplified sandwich assay with ambient O-2 as the substrate. *Anal. Chem.* **76,** 4093–4097 (2004).
25. Möller, R., Powell, R. D., Hainfeld, J. F. & Fritzsche, W. Enzymatic control of metal deposition as key step for a low-background electrical detection for DNA chips. *Nano Lett.* **5,** 1475–1482 (2005).

Acknowledgements

We wish to acknowledge Genome Canada, the Ontario Ministry of Innovation and Research, the Ontario Centres of Excellence, Ontario Institute for Cancer Research, Canada Foundation for Innovation, Canadian Institutes of Health Research, and NSERC for their support of this work. We also acknowledge X. Sun for his contributions to the optimization of electrodeposition conditions.

Author contributions

L.S., Z.F., E.H.S. and S.O.K. conceived and designed the experiments; L.S. and Z.F. performed the experiments; L.S. and Z.F. analysed the data. All authors discussed the results and co-wrote and commented on the manuscript.

Additional information

Supplementary information accompanies this paper at www.nature.com/naturenanotechnology. Reprints and permission information is available online at http://npg.nature.com/reprintsandpermissions/. Correspondence and requests for materials should be addressed to E.H.S. and S.O.K.